




Extracting the central positions and widths of Fano-type tunneling channels in a spectrum from the ionization rate

Lijuan Jia ^{1,2} Wei-Chao Jiang,¹ Haijun Xing ^{3,*} and Libin Fu ^{2,†}¹*Institute of Quantum Precision Measurement, College of Physics and Optoelectronic Engineering, Shenzhen University, Shenzhen 518060, China*²*Graduate School of China Academy of Engineering Physics, No. 10 Xibeiwang East Road, Haidian District, Beijing 100193, China*³*Center for Quantum Sciences and School of Physics, Northeast Normal University, Changchun 130024, China*

(Received 1 February 2023; revised 4 April 2023; accepted 14 July 2023; published 27 July 2023)

The spectrum of a bound state plays a crucial role in the field-induced tunneling ionization, as ionization is essentially a dressing dissipative process. Based on the Fano-resonance theory, a single Lorentzian spectrum can be approximately obtained for each bound state. The coupling transition between bound states enriches the spectrum and complicates the tunneling dynamics. Previous attempts to extract the spectrum characteristics of the tunneling system from the ionization rate required an artificial filter function, and only the spectrum characteristics of the ground state can be obtained. In this study, we achieve a two-level model by parametrizing the main peaks of the spectrum with a Lorentzian function. This model successfully reproduces the ionization rate. By matching the central positions and widths of the Fano-type peaks with the behaviors of the ionization rate, we establish the relations between the model parameters and the details of the spectral peaks, namely, the Fano-type peaks. Our work introduces a systematic method to obtain key information of the spectrum, which can be generalized to multiple-level systems.

DOI: [10.1103/PhysRevA.108.013119](https://doi.org/10.1103/PhysRevA.108.013119)

I. INTRODUCTION

Field-induced tunneling ionization of atoms serves as the cornerstone of many strong-field physical phenomena. Progress in attosecond technology has allowed for deeper explorations of the ultrafast tunneling dynamics of electrons. Remarkably, a tens-of-attosecond time required for an electron tunneling process is measured in attoclock experiments [1,2], which brings many confirmations or disputes about the measured time [3–7]. Previously, tunneling ionization has been regarded as a direct transition from the ground state to free-electron states, treated within the framework of the strong-field approximation (SFA) [8–10]. Only recently, an ionization channel in which electrons transition to continuum via excited-bound states or virtual transient electronic states has been found theoretically [11–15]. This discovered channel complicates the dynamical process of tunneling ionization. Meanwhile, attosecond spectroscopy has also been applied to study electronic motion in real time. For example, it has enabled the observation of a few-femtosecond Auger process [16], as well as the first experimental evidence for ionization steps in field-induced electron tunneling [17]. In particular, by virtue of the high sensitivity of attosecond transient absorption spectroscopy (ATAS) [18–20], the real-time excited-state populations are measured experimentally [21]. This suggests the possibility of probing the multiple-channel tunneling process in experiment.

Tunneling ionization is essentially a dissipative process, in which the initial populations of bound states are gradually depleted. Since multiple bound states are involved in the ionization process [11–15], figuring out the dissipative characteristics and the role of each bound state become vital in revealing the tunneling dynamics, which is complicated by the transition couplings of bound states. The quantum method of the time-dependent Schrödinger equation (TDSE) [6,7,22–24] provides a simulation that captures all the details of the entire ionization process. Other commonly used methods such as SFA, hybrid quantum-classical backpropagation [25–27], semiclassical three-step models [28,29], and classical methods [30] pay little attention to the behaviors of bound states.

Generally, Fano theory [31,32] provides a framework for dealing with the dissipative dynamical process of tunneling systems. It shows that the Fano-type channel of the spectrum determines the tunneling process and the lifetime of bound states. The inner decisive relations can be connected by ionization rate $w(t)$. MacDonald *et al.* [11] have studied $w(t)$ and obtained that the steady value of $w(t)$ is the width of the filtered ground-state Fano-type channel. However, the artificially removed coupling interactions of bound states prevented the establishment of further relations. In our recent work [15], we found that the effect of bound-state couplings on tunneling dynamics is non-negligible. The presence of excited-state tunneling channels further confirms the important role of coupling interactions [12,15]. Nevertheless, the phenomenological approach employed in our study [15] yields that we have barely contributed to extracting dynamical information from $w(t)$.

*hjxing3@icloud.com

†lbfu@gscaep.ac.cn

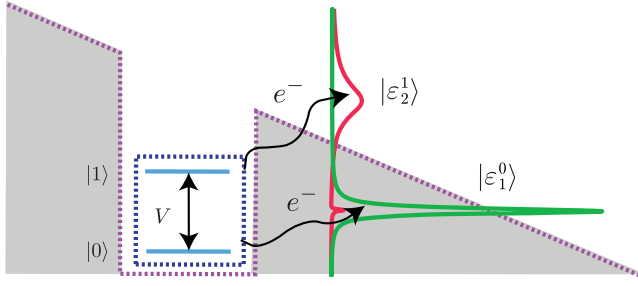


FIG. 1. The sketch of electron tunneling and Fano-type tunneling channels.

In this work, by selecting the main peaks in the spectra, we deduce a two-level leakage model. This model allows us to extract the primary *dissipative characteristics*, i.e., the central positions and widths of the Fano-type tunneling channels, from the ionization rate. Since the dynamic characteristics of the system are encoded into the parameters of the model, we obtain the Fano-type peaks in the spectra ruling tunneling process by diagonalizing the model. Hence, an explicit image of tunneling dynamical behaviors of electrons inside the atom is presented, as shown in Fig. 1. Atomic units are used throughout the paper, unless stated otherwise.

II. FORMULATION

Tunneling ionization refers to the process where electrons within an atom escape from the binding potential suppressed by an external field. The atom is initially in its ground state, and the Hamiltonian of this perturbed system described in the length gauge is

$$H = H_0 - \mathbf{r} \cdot \mathbf{F}, \quad (1)$$

where $H_0 = T + V$, with T the kinetic energy, V the bare potential, and \mathbf{F} a static electric field switching on at time $t = 0$. In the presence of this external field, the bound state is diluted to a band with a finite width that determines its lifetime. Inspired by Fano theory [31,32], the width can be estimated by calculating the spectral density $|g_n(\varepsilon)|^2$ of the bound state, which is

$$|g_n(\varepsilon)|^2 = |\langle n | \varphi_\varepsilon \rangle|^2, \quad (2)$$

where $|n\rangle$ is a discrete eigenstate of H_0 with eigenenergy E_n , and $n = 0, 1, 2, \dots$. Also, ε and $|\varphi_\varepsilon\rangle$ are the eigenvalues and eigenstates of H .

Traditionally, Fano theory describes a simplified dissipative system H_F ,

$$H_F = \sum_n E_n |n\rangle \langle n| + \int d\omega \omega |\omega\rangle \langle \omega| + \int d\omega \sum_n W_n [|\omega\rangle \langle n| e^{-i\varphi_n} + \text{H.c.}], \quad (3)$$

where only the direct couplings between the bound state and continuum of H_0 are considered. W_n is the coupling coefficient of the n th bound state with the continuum. $|\omega\rangle$ is the continuum eigenstate of H_0 with energy ω . It can be solved analytically by assuming W_n independent of ω . The spectral

density of the bound state in the system H_F is given by

$$|g_n^F(\varepsilon')|^2 = \frac{W_n^2 z(\varepsilon')^2}{(\varepsilon' - E_n)^2 [\pi^2 + z(\varepsilon')^2]}, \quad (4)$$

where $z(\varepsilon') = (\sum_n \frac{W_n^2}{\varepsilon' - E_n})^{-1}$, with ε' the eigenenergy of H_F . In the regime of weak coupling, $|g_n^F(\varepsilon')|^2$ approximately follows a Lorentzian distribution, for it only has one major peak with the width much smaller than the energy gap between discrete states. This single prominent peak suggests a Fano-type dissipative channel and its width gives the depletion rate of the n th discrete state.

In realistic tunneling dynamics, the additional coupling terms between bound states, which are not accounted for in H_F , can have a significant impact. This effect enriches the spectrum rather than a single Lorentzian peak, and the resulting tunneling dynamics becomes complicated. McDonald *et al.* [11] studied the system H , but filtered transition couplings. We considered the effects of these coupling terms and found that $w(t)$ can be roughly described by a finite-level model [15]. This model is phenomenological. The parameters of the model are determined by fitting the results obtained from solving the TDSE. Thus, the physics encoded in the parameters is not explicitly clear, limiting our ability to extract dynamical information of tunneling electrons from $w(t)$ with the aid of the model.

Indeed, the spectrum carries dissipative information of the bound state, allowing us to improve the previous phenomenological model from the spectrum itself. By this improved model, we eventually uncover the tunneling dynamical process of electrons and obtain the dissipative characteristics of the tunneling system from $w(t)$. Specifically, from the time-dependent generalization of Fano-resonance theory [31], $w(t)$ reads [15]

$$w(t) = \frac{\iint d\varepsilon_1 d\varepsilon_2 i(\varepsilon_1 - \varepsilon_2) e^{-i(\varepsilon_1 - \varepsilon_2)t} G_{12}(\varepsilon_1, \varepsilon_2)}{\iint d\varepsilon_1 d\varepsilon_2 e^{-i(\varepsilon_1 - \varepsilon_2)t} G_{12}(\varepsilon_1, \varepsilon_2)}, \quad (5)$$

with $G_{12}(\varepsilon_1, \varepsilon_2) = g_0(\varepsilon_1) g_0^*(\varepsilon_2) \sum_n g_n(\varepsilon_1) g_n^*(\varepsilon_2)$. Equation (5) is defined in the length gauge, which corresponds to the actual ionization rate. We mention that time-dependent ionization probability is gauge invariant on the condition that the definition of the ionization is unambiguous and consistent in different gauges. For the velocity gauge, the same ionization rate can be derived via a resolvent operator method [33].

In our investigation, we use a one-dimensional (1D) square-well potential and model the tunneling potential $V_{\text{eff}}(x) = V - \mathbf{r} \cdot \mathbf{F}$ as

$$V_{\text{eff}}(x) = \begin{cases} -V_0 & \text{for } |x| < a \\ -xF & \text{otherwise.} \end{cases} \quad (6)$$

V_0 and $2a$ are the depth and width of the bare potential. With setting $V_0 = 2$ and $a = 1.5$, H_0 contains two bound states $|0\rangle$ and $|1\rangle$. In this case, $g_n(\varepsilon)$ is a real number.

For rough comparison, we also apply Fano theory to describe the square-well potential system. At $F = 0.40$, we depict the spectral densities $|g_n(\varepsilon)|^2$ and $|g_n^F(\varepsilon')|^2$ in Fig. 2. In the realistic situation, the coupling coefficient $W_n(\omega)$ of the n th discrete state to the continuum is dependent on ω .

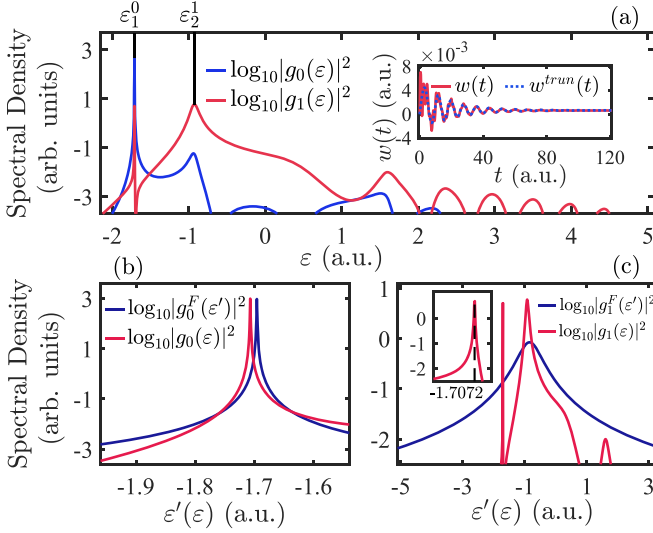


FIG. 2. (a) Spectral densities as a function of ε . ε_1^0 is the central energy of the first peak of $|g_0(\varepsilon)|^2$, and ε_2^1 is the central energy of the second peak of $|g_1(\varepsilon)|^2$. The inset shows untruncated $w(t)$ and truncated $w^{\text{trunc}}(t)$. (b) [(c)] Spectral density $|g_0^F(\varepsilon')|^2$ [$|g_1^F(\varepsilon')|^2$] as a function of ε' . For comparison, $|g_0(\varepsilon)|^2$ [$|g_1(\varepsilon)|^2$] is also presented for the same energy range. The inset in (c) magnifies the first peak of $|g_1(\varepsilon)|^2$. Here, $F = 0.40$ a.u.

In the case of Fano theory, we take $W_n = \max_{\omega} [W_n(\omega)]$, resulting in $W_1 = 0.0104$ and $W_2 = 0.3462$. It is reasonable to take the coupling coefficient as a constant since the spectral width of the bound state is much narrower than the width of $W_n(\omega)$. Compared to the single Lorentzian peak of Fano theory (see Fig. 2), additional couplings in H trigger small peaks near the Fano-type resonant peak (channel) centered at ε_1^0 (ε_2^1). These additional couplings also distort the shape of the spectral distribution, deviating from a Lorentzian distribution. Furthermore, the energy-dependent coefficient $W_n(\omega)$ shifts the central positions of the resonant peaks [Figs. 2(b) and 2(c)].

III. TWO-LEVEL MODEL

Owing to the coupling transitions, the whole spectrum contributes to the tunneling dynamics, while the main features of $w(t)$ can be captured by retaining only the low-energy part of the spectrum. After calculating with different truncations of the energy, we find that the main contributions to $w(t)$ come from the negative-energy part of the spectrum. Namely, as shown in the inset of Fig. 2(a), the long-time behaviors of $w(t)$ can be reproduced by retaining only the negative-energy part of the spectrum. In this negative-energy range, there are only four peaks [two peaks of $|g_0(\varepsilon)|^2$ and the other two peaks of $|g_1(\varepsilon)|^2$] [see Fig. 2(a)]. To capture the leading-order contributions (the position and width of the peak), we take each of these four peaks as a Lorentzian distribution, which means we introduce four channels with constant lifetimes.

We first express the electron wave function at time t as

$$|\psi(t)\rangle = c_0(t)|0\rangle + c_1(t)|1\rangle + \int c_{\omega}(t)|\omega\rangle d\omega, \quad (7)$$

where $c_0(t)$, $c_1(t)$, and $c_{\omega}(t)$ are the probability amplitudes. At $t = 0$, $c_0 = 1$ and other probability amplitudes are zero. Expanding $|0\rangle = \int d\varepsilon g_0(\varepsilon)|\varphi_{\varepsilon}\rangle$ and $|1\rangle = \int d\varepsilon g_1(\varepsilon)|\varphi_{\varepsilon}\rangle$, and projecting $\langle 0|$ and $\langle 1|$ on the left-hand side of Eq. (7), we have the evolution of (c_0, c_1) in matrix form,

$$\begin{pmatrix} c_0(t) \\ c_1(t) \end{pmatrix} = \tilde{U}(t, t') \begin{pmatrix} c_0(t') \\ c_1(t') \end{pmatrix}, \quad (8)$$

with

$$\tilde{U}(t, t') = \begin{pmatrix} \int d\varepsilon e^{-i\varepsilon(t-t')} |g_0(\varepsilon)|^2 & \int d\varepsilon e^{-i\varepsilon(t-t')} g_0(\varepsilon)g_1(\varepsilon) \\ \int d\varepsilon e^{-i\varepsilon(t-t')} g_0(\varepsilon)g_1(\varepsilon) & \int d\varepsilon e^{-i\varepsilon(t-t')} |g_1(\varepsilon)|^2 \end{pmatrix}.$$

In further calculations, we approximate the first two peaks of the spectra $|g_0(\varepsilon)|^2$ ($|g_1(\varepsilon)|^2$) by a sum of two Lorentzian functions. Simultaneously, the cross term $g_0(\varepsilon)g_1(\varepsilon)$ is determined. For convenience and simplicity, we also fit $g_0(\varepsilon)g_1(\varepsilon)$ with a sum of two Lorentzian functions, where the leading-order contributions of $g_0(\varepsilon)g_1(\varepsilon)$ are included. Note that the fitted Lorentzian parameters of $g_0(\varepsilon)g_1(\varepsilon)$ are dependent of $|g_0(\varepsilon)|^2$ and $|g_1(\varepsilon)|^2$. The Lorentzian function is defined as $L(A_k^j, \gamma_k^j, \varepsilon_k^j) = A_k^j \frac{(\gamma_k^j/2)^2}{(\gamma_k^j/2)^2 + (\varepsilon - \varepsilon_k^j)^2}$, where $k = 1, 2$ and $j = 0, 1, 2$ represent the spectra $|g_0(\varepsilon)|^2$, $|g_1(\varepsilon)|^2$, and $g_0(\varepsilon)g_1(\varepsilon)$, respectively. The parameters $(A_k^j, \gamma_k^j, \varepsilon_k^j)$ are the peak value, the width, and the central energy of the k th peak of the spectrum j . Subsequently, $\tilde{U}(t, 0)$ becomes, accordingly,

$$\tilde{U}(t, 0) = \begin{pmatrix} a_1^0 f_1^0(t) + a_2^0 f_2^0(t) & a_1^2 f_1^2(t) + a_2^2 f_2^2(t) \\ a_1^2 f_1^2(t) + a_2^2 f_2^2(t) & a_1^1 f_1^1(t) + a_2^1 f_2^1(t) \end{pmatrix},$$

with $a_k^j = A_k^j \pi \frac{\gamma_k^j}{2}$, $f_k^j(t) = e^{-i\varepsilon_k^j t - \frac{\gamma_k^j}{2} t}$.

We then have the unionized electron wave function, which is given by

$$|\tilde{\psi}(t)\rangle = c_0(t)|0\rangle + c_1(t)|1\rangle. \quad (9)$$

Equation (9) satisfies the TDSE, from which we obtain a partial Hamiltonian,

$$\begin{aligned} \tilde{H}(t) &= i\partial_t \tilde{U}(t, 0) \tilde{U}^{-1}(t, 0), \\ &\equiv \begin{pmatrix} E_1(t) - i\Gamma_1(t)/2 & V_1(t) + iV_2(t) \\ V_3(t) + iV_4(t) & E_2(t) - i\Gamma_2(t)/2 \end{pmatrix}. \end{aligned} \quad (10)$$

This partial Hamiltonian can be equivalently regarded as a result of tracing over the continuum states. For clarity and readability, a detailed expression of $\tilde{H}(t)$ is given in Appendix A. In fact, we have recently found that the main behaviors of $w(t)$ can be roughly described by a time-independent two-level Hamiltonian [15]. We thus perform a time average on $\tilde{H}(t)$ as $\bar{H} = \frac{1}{T} \int_0^T \tilde{H}(t) dt$. From Magnus expansion [34], this average treatment is equivalent to making an approximation that $\tilde{H}(t)$ at different times are commutative, and we finally get

$$\bar{H} = \begin{pmatrix} E_1 - i\Gamma_1/2 & V_1 + iV_2 \\ V_3 + iV_4 & E_2 - i\Gamma_2/2 \end{pmatrix}, \quad (12)$$

which is just the improved two-level model. T can be infinite, in principle. But, for very large T , the probability of the electron populating on the excited state becomes extremely small. This can lead to numerical errors and distorts the results. Furthermore, the specific dynamics that we focus on is

the duration during which the wave function reaches a steady state, where $w(t)$ approaches a steady value. Hence, we select T that is around the steady-state time.

This improved two-level Hamiltonian \bar{H} is directly deduced from the spectrum, so that the main characteristics of the tunneling system are naturally encoded into \bar{H} . This distinguishes it from the previous model [15]. Similar to $w(t)$ [Eq. (5)], we obtain a leakage rate $w_L(t)$ from the model \bar{H} . $w_L(t)$ is given by

$$w_L(t) = -\frac{\partial_t [|\bar{c}_1(t)|^2 + |\bar{c}_2(t)|^2]}{|\bar{c}_1(t)|^2 + |\bar{c}_2(t)|^2}, \quad (13)$$

with $\bar{c}_1(t)$ and $\bar{c}_2(t)$ denoting the probability amplitudes of the two states in \bar{H} . At a fixed field F , $w_L(t)$ is a known expression that solely depends on time t . Straightforwardly, we compare $w_L(t)$ with $w(t)$ [Eq. (5)] for different F in Appendix B. The results demonstrate a remarkable agreement between $w_L(t)$ and $w(t)$ for long times. One can see that the ionization rate is negative at certain times. This arises from the fact that electrons populated on the continuum will flow back to bound states. For further support, we have discussed the consistency of the results for choosing different T at $F = 0.30$ a.u. in Appendix C. Therefore, we can conclude that model \bar{H} is highly effective in reproducing the primary tunneling dynamics of electrons.

IV. POSITION AND WIDTH OF THE FANO-TYPE CHANNEL

To further analyze the main dynamical characteristics of tunneling electrons from the well-defined two-level leakage model, we calculate the eigenvalues of \bar{H} and denote them as $\lambda_1 = \bar{E}_1 - i\bar{\Gamma}_1/2$ and $\lambda_2 = \bar{E}_2 - i\bar{\Gamma}_2/2$. Here, \bar{E}_1 and \bar{E}_2 are the central positions of the eigenchannels of the tunneling electrons, and $\bar{\Gamma}_1$ and $\bar{\Gamma}_2$ are the corresponding widths. These two eigenchannels dominate the tunneling behavior of electrons. Note that the four sharp peaks in the spectra [Fig. 2(a)] play the major role in the tunneling process. To figure out the relationship between these four sharp peaks and the two tunneling eigenchannels, we compare them in Fig. 3. For weak fields, we observe that $\bar{E}_1 \approx \varepsilon_1^0 \approx \varepsilon_1^1$, $\bar{E}_2 \approx \varepsilon_2^0 \approx \varepsilon_2^1$, $\bar{\Gamma}_1 \approx \gamma_1^0 \approx \gamma_1^1$, and $\bar{\Gamma}_2 \approx \gamma_2^0 \approx \gamma_2^1$. In this case, the four sharp peaks in the spectra correspond to the two tunneling channels. Namely, the two tunneling eigenchannels correspond to the two Fano-type peaks in the spectra. However, for stronger fields, these relations no longer hold. Particularly, ε_2^0 largely deviates from ε_2^1 , while \bar{E}_2 eventually approaches ε_2^1 . As a result, the relations become $\bar{E}_1 \approx \varepsilon_1^0$, $\bar{\Gamma}_1 \approx \gamma_1^0$ and $\bar{E}_2 \approx \varepsilon_2^1$, $\bar{\Gamma}_2 \approx \gamma_2^1$. From these behaviors, we conclude that the two eigenchannels derived from our model are the two Fano-type channels in the spectra. This shows that though coupling interactions complicate the spectra and tunneling signals of electrons, Fano-type peaks still dominate the tunneling dynamics of electrons. Furthermore, this result establishes an explicit physical correspondence for each parameter in the improved model after diagonalization, rendering the model no longer phenomenological.

This physical coincidence of the eigenchannels from the model and the Fano-type channels in the spectra presents a clear tunneling image of the electron inside the atom, as

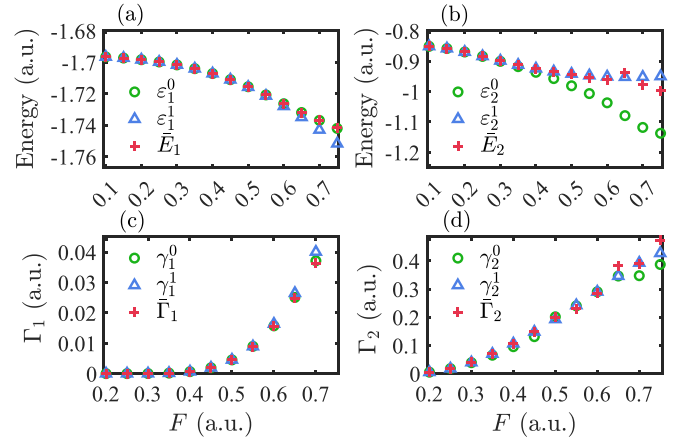


FIG. 3. (a) [(b)] The energy as a function of the field F . ε_1^0 [ε_2^0] and ε_1^1 [ε_2^1] are central energies of the first [second] peak of spectra $|g_0(\varepsilon)|^2$ and $|g_1(\varepsilon)|^2$. \bar{E}_1 and \bar{E}_2 are eigenchannels. (c) [(d)] The width as a function of F . γ_1^0 [γ_2^0] and γ_1^1 [γ_2^1] are the widths of the first [second] peak of spectra $|g_0(\varepsilon)|^2$ and $|g_1(\varepsilon)|^2$. $\bar{\Gamma}_1$ and $\bar{\Gamma}_2$ are band widths of the eigenchannels.

depicted in Fig. 1. The electron initially populates on the bare state $|0\rangle$. Due to the coupling interactions, electrons are transitioned to the first excited state. These coherent electrons then escape from the trap barrier, predominately via two Fano-type tunneling channels, namely, the ground-state resonance channel and the excited-state resonance channel. These channels are composed of a group of dressed states centered at ε_1^0 and ε_2^1 , respectively. In the weak-field limit, the central positions of the two Fano-type channels coincide with those calculated by Fano theory.

Now, we can explain the temporal behaviors of $w(t)$. The oscillation observed in $w(t)$ is mainly caused by the interference of the initial propagating waves from the two Fano-type tunneling channels. Since $\gamma_2^1 \gg \gamma_1^0$ and the population on the

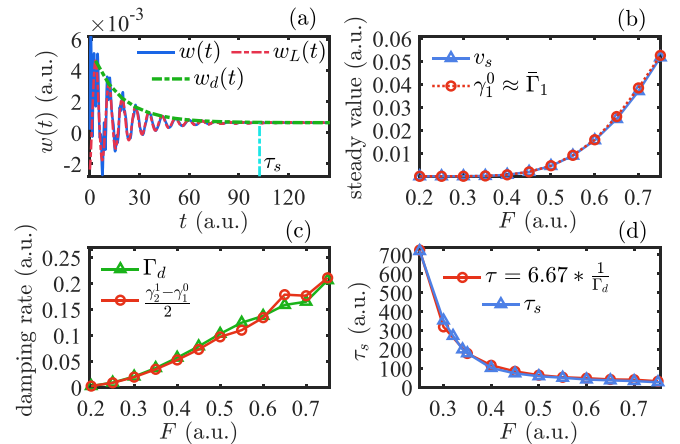


FIG. 4. (a) Ionization rate $w(t)$ [Eq. (5)] and $w_L(t)$ [Eq. (13)]. $w_d(t)$ is the damping curve. τ_s is the steady time of $w(t)$. It is determined at which the relative error is 1% of its steady-state value. Here, $F = 0.40$. (b) Steady value, (c) damping rate, and (d) steady time τ_s as a function of F .

excited state $|1\rangle$ becomes extremely small for longer times, $w(t)$ approaches a steady value denoted as v_s .

When the spectra of the bound states are unknown beforehand, we can extract the spectral information of dominating tunneling dynamics of the electron (namely, the positions and widths of the Fano-type tunneling channels) from the behaviors of $w(t)$ with the help of our constructed model. The extraction process can be outlined as follows:

(1) $w(t)$ oscillates with a damping amplitude [green line in Fig. 4(a)], marked as $w_d(t)$. From our model [Eq. (13)], we first deduce (see Appendix D)

$$\begin{aligned} w_d(t) &\approx Ae^{-\frac{\Gamma_2-\Gamma_1}{2}t} + \bar{\Gamma}_1 \\ &= Ae^{-\frac{\gamma_2^1-\gamma_1^0}{2}t} + \gamma_1^0. \end{aligned} \quad (14)$$

Based on Eq. (14), the damping curve can be expressed in a general form as $w_d(t) = Ae^{-\Gamma_d t} + v_s$. Here, v_s is the steady value of $w(t)$ and can be directly read from the TDSE results. The damping rate Γ_d is determined by fitting with $w(t)$ calculated by TDSE. We compare v_s with γ_1^0 ($\gamma_1^0 \approx \bar{\Gamma}_1$) in Fig. 4(b) and plot Γ_d and $\frac{\gamma_2^1-\gamma_1^0}{2}$ ($\frac{\gamma_2^1-\gamma_1^0}{2} \approx \frac{\Gamma_2-\Gamma_1}{2}$) in Fig. 4(c). It is evident that they are in good agreement. We can directly infer that $\gamma_1^0 \approx v_s$ and $\gamma_2^1 \approx 2\Gamma_d + v_s$. Hence, we are able to obtain the widths of the Fano-type channels in the spectra. These consistent results again validate the rationality of the Lorentzian-spectrum approximation.

(2) The oscillation period \mathcal{T} of $w(t)$ is related to the energy gap $\delta\varepsilon$ ($\delta\varepsilon = \varepsilon_2^1 - \varepsilon_1^0 \approx \bar{E}_2 - \bar{E}_1$) of the two Fano-type resonance tunneling channels. Specifically, from Eq. (D2), the relation is $\mathcal{T} = 2\pi/\delta\varepsilon$. In the tunneling ionization regime ($F \leq 0.56$ a.u.), the oscillation period \mathcal{T} increases with the increase of the external field. By extracting \mathcal{T} from $w(t)$, we can determine the relative position of the two Fano-type channels.

The magnitude of $w_d(t)$ reflects the coherence degree of the two Fano-type channels. The oscillation duration of $w(t)$ is determined by the excited-state resonance channel due to $\gamma_2^1 \gg \gamma_1^0$. Moreover, we identify the steady time of $w(t)$ as τ_s [Fig. 4(a)]. τ_s is determined at which the relative error is 1% of the steady-state value. The damping rate Γ_d suggests the value of τ_s . As shown in Fig. 4(d), τ_s is approximately proportional to Γ_d inversely; specifically, $\tau_s \approx 6.67 * \frac{1}{\Gamma_d} \approx 13.34 * \frac{1}{\gamma_2^1-\gamma_1^0}$.

V. CONCLUSION AND DISCUSSION

The spectrum plays a crucial role in the study of perturbed systems as it can reveal many characteristics of the perturbed systems. In particular, the spectral width accounts for the lifetime of a metastable state. This is a common concern in various fields. In the complicated tunneling process involving multiple bound states, we have developed a systematic method to extract the spectral key information from the ionization rate in the context of strong-field perturbation with the aid of a constructed two-level model. Our method is also applicable for multiple-level systems and the case of weak-coupling limit [11,32]. For generalized cases, one can get the spectral key information according to the extraction steps (1) and (2) outlined in Sec. IV. We have actually suggested a perspective that one can infer tunneling dynamics by measuring the ionization rate, opening up a different avenue for studying tunneling dynamics of electrons.

Furthermore, in the strong-field regime, a significant Stark shift and the coupling to the continuum distinguish our model from Rabi oscillation [35], which describes the dynamical process of a two-level system perturbed by an extremely weak external field. Specifically, the period oscillation of ionization rate behaves differently from the Rabi period, which decreases with the increase of the field. The coupling to the continuum introduces an exponential decay to the system. Note that our constructed model will reduce to Rabi oscillation in the weak-field limit.

In recent years, ATAS has enabled the measurement of the real-time populations of transient states [21]. Additionally, a recent study by Jiang *et al.* [36] successfully retrieved the time-dependent populations of bound states from the ionization spectra. We anticipate that the advances in attosecond techniques will allow for the measurement of $w(t)$ in the future. We think our work significantly contributes to the study of electron tunneling dynamics.

ACKNOWLEDGMENTS

This work was supported by the National Natural Science Foundation of China (Grants No. 11725417, No. 12088101, No. 12047548, No. 12074265 and No. U1930403), Science Challenge Project (Grant No. TZ2018005), and Guangdong Basic and Applied Basic Research Foundation (Grant No. 2022A1515010329).

APPENDIX A: THE DERIVATION OF THE PARTIAL HAMILTONIAN $\tilde{H}(t)$

After some straightforward calculations, the Hamiltonian $\tilde{H}(t)$ [Eq. (10)] ends up with

$$\tilde{H}(t) = i \frac{1}{|\tilde{U}|} \begin{pmatrix} b_1^0 f_1^0(t) + b_2^0 f_2^0(t) & b_1^1 f_1^1(t) + b_2^1 f_2^1(t) \\ b_1^2 f_1^2(t) + b_2^2 f_2^2(t) & b_1^1 f_1^1(t) + b_2^1 f_2^1(t) \end{pmatrix} \begin{pmatrix} a_1^1 f_1^1(t) + a_2^1 f_2^1(t) & -a_1^2 f_1^2(t) - a_2^2 f_2^2(t) \\ -a_1^2 f_1^2(t) - a_2^2 f_2^2(t) & a_1^0 f_1^0(t) + a_2^0 f_2^0(t) \end{pmatrix}, \quad (A1)$$

where $a_k^j = A_k^j \pi \frac{\gamma_k^j}{2}$, $f_k^j(t) = e^{-i\varepsilon_k^j t - \frac{\gamma_k^j}{2} t}$, $b_k^j = -i(\varepsilon_k^j - i\frac{\gamma_k^j}{2})a_k^j$, $|\tilde{U}| = [a_1^0 f_1^0(t) + a_2^0 f_2^0(t)][a_1^1 f_1^1(t) + a_2^1 f_2^1(t)] - [a_1^2 f_1^2(t) + a_2^2 f_2^2(t)]^2$, $k = 1, 2$, $j = 0, 1, 2$, respectively. For more clearness, we list the four matrix elements of $\tilde{H}(t)$ as follows:

$$\begin{aligned} |\tilde{U}| \tilde{H}_{11} &= [(A_1^1 + A_2^1)(\mathcal{A}_1^0 \varepsilon_1^0 + \mathcal{A}_2^0 \varepsilon_2^0) - (A_1^2 + A_2^2)(\mathcal{A}_1^2 \varepsilon_1^2 + \mathcal{A}_2^2 \varepsilon_2^2)] \\ &\quad - i \frac{1}{2} [(A_1^1 + A_2^1)(\mathcal{A}_1^0 \gamma_1^0 + \mathcal{A}_2^0 \gamma_2^0) - (A_1^2 + A_2^2)(\mathcal{A}_1^2 \gamma_1^2 + \mathcal{A}_2^2 \gamma_2^2)], \end{aligned} \quad (A2)$$

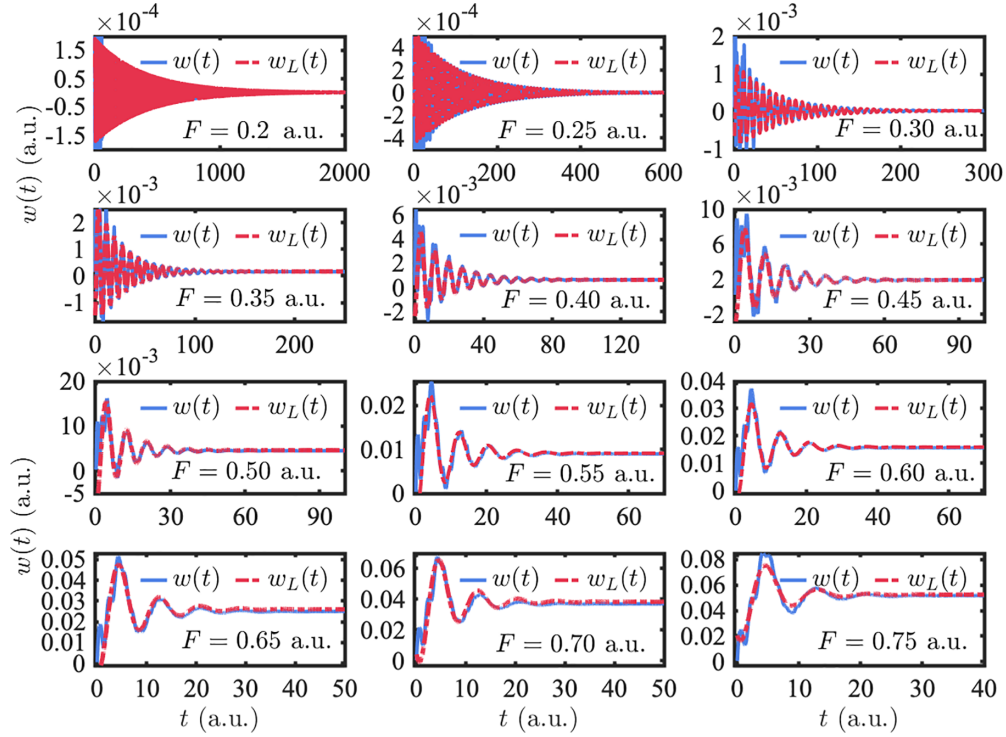


FIG. 5. $w(t)$ and $w_L(t)$ as a function of t . Blue line is the result of the TDSE. Red line is the result of the model.

with $\mathcal{A}_k^j = a_k^j f_k^j(t)$, $k = 1, 2$, $j = 0, 1, 2$, respectively.

$$\begin{aligned} |\tilde{U}|\tilde{H}_{12} = & [-(\mathcal{A}_1^2 + \mathcal{A}_2^2)(\mathcal{A}_1^0 \varepsilon_1^0 + \mathcal{A}_2^0 \varepsilon_2^0) + (\mathcal{A}_1^0 + \mathcal{A}_2^0)(\mathcal{A}_1^2 \varepsilon_1^2 + \mathcal{A}_2^2 \varepsilon_2^2)] \\ & - i\frac{1}{2}[-(\mathcal{A}_1^2 + \mathcal{A}_2^2)(\mathcal{A}_1^0 \gamma_1^0 + \mathcal{A}_2^0 \gamma_2^0) + (\mathcal{A}_1^0 + \mathcal{A}_2^0)(\mathcal{A}_1^2 \gamma_1^2 + \mathcal{A}_2^2 \gamma_2^2)], \end{aligned} \quad (\text{A3})$$

$$\begin{aligned} |\tilde{U}|\tilde{H}_{21} = & [(\mathcal{A}_1^1 + \mathcal{A}_2^1)(\mathcal{A}_1^2 \varepsilon_1^2 + \mathcal{A}_2^2 \varepsilon_2^2) - (\mathcal{A}_1^2 + \mathcal{A}_2^2)(\mathcal{A}_1^1 \varepsilon_1^1 + \mathcal{A}_2^1 \varepsilon_2^1)] \\ & - i\frac{1}{2}[(\mathcal{A}_1^1 + \mathcal{A}_2^1)(\mathcal{A}_1^2 \gamma_1^2 + \mathcal{A}_2^2 \gamma_2^2) - (\mathcal{A}_1^2 + \mathcal{A}_2^2)(\mathcal{A}_1^1 \gamma_1^1 + \mathcal{A}_2^1 \gamma_2^1)], \end{aligned} \quad (\text{A4})$$

$$\begin{aligned} |\tilde{U}|\tilde{H}_{22} = & [-(\mathcal{A}_1^2 + \mathcal{A}_2^2)(\mathcal{A}_1^2 \varepsilon_1^2 + \mathcal{A}_2^2 \varepsilon_2^2) + (\mathcal{A}_1^0 + \mathcal{A}_2^0)(\mathcal{A}_1^1 \varepsilon_1^1 + \mathcal{A}_2^1 \varepsilon_2^1)] \\ & - i\frac{1}{2}[-(\mathcal{A}_1^2 + \mathcal{A}_2^2)(\mathcal{A}_1^2 \gamma_1^2 + \mathcal{A}_2^2 \gamma_2^2) + (\mathcal{A}_1^0 + \mathcal{A}_2^0)(\mathcal{A}_1^1 \gamma_1^1 + \mathcal{A}_2^1 \gamma_2^1)]. \end{aligned} \quad (\text{A5})$$

Finally, we simply express $\tilde{H}(t)$ as

$$\tilde{H}(t) \equiv \begin{pmatrix} E_1(t) - i\Gamma_1(t)/2 & V_1(t) + iV_2(t) \\ V_3(t) + iV_4(t) & E_2(t) - i\Gamma_2(t)/2 \end{pmatrix}. \quad (\text{A6})$$

The parameters in $\tilde{H}(t)$ are the function of the characteristic quantities of the peaks.

APPENDIX B: THE IONIZATION RATE $w_L(t)$ AND $w(t)$

We compare $w_L(t)$ and $w(t)$ in Fig. 5 for different field strengths F . In a wide range of field, $w_L(t)$ derived from our model coincides well with $w(t)$ calculated from the TDSE for long times.

APPENDIX C: THE CONVERGENCY OF THE RESULTS FOR CHOOSING DIFFERENT T

For $F = 0.30$ a.u., the time of $w(t)$ approaching a steady value is around 250 a.u. We have, respectively, selected $T = 150, 200, 250, 300$ a.u. to check the consistency of the results,

as shown in Fig. 6. We can see clearly that for long times, $w_L(t)$ coincides with $w(t)$ for different T .

APPENDIX D: THE DAMPING CURVE $w_d(t)$

We mark the eigenvalues of \bar{H} as $\lambda_1 = \bar{E}_1 - i\bar{\Gamma}_1/2$ and $\lambda_2 = \bar{E}_2 - i\bar{\Gamma}_2/2$ and the eigenvectors as $|v_1\rangle$ and $|v_2\rangle$. \bar{H} is non-Hermitian; thereby, $|v_1\rangle$ and $|v_2\rangle$ are complex vectors and not orthogonal. The ionized wave function of the electrons can be given by

$$|\tilde{\psi}(t)\rangle = c_1 e^{-i\lambda_1 t} |v_1\rangle + c_2 e^{-i\lambda_2 t} |v_2\rangle, \quad (\text{D1})$$

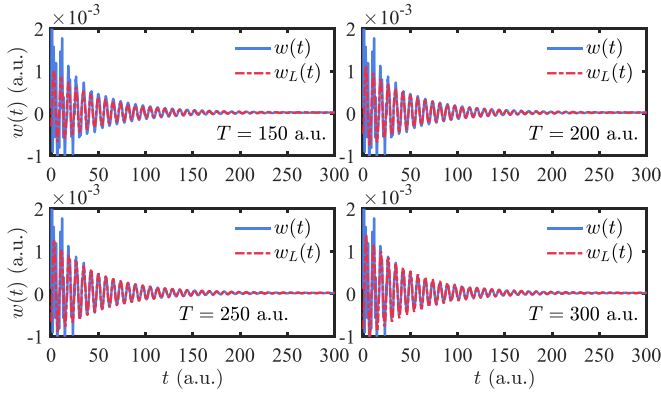


FIG. 6. $w(t)$ and $w_L(t)$ as a function of t . The blue line and red line are the results of the TDSE and model, respectively, for different T .

where c_1 and c_2 are the initial amplitudes. $(c_1, c_2) \in \mathbb{R}^2$, and $\bar{\Gamma}_2 \gg \bar{\Gamma}_1$. Then,

$$\begin{aligned} \langle \tilde{\psi}(t) | \tilde{\psi}(t) \rangle &= c_1^2 e^{-\bar{\Gamma}_1 t} + c_2^2 e^{-\bar{\Gamma}_2 t} + c_1 c_2 \langle v_1 | v_2 \rangle |e^{-\frac{\bar{\Gamma}_1 + \bar{\Gamma}_2}{2} t} \\ &\times [e^{i(\bar{E}_1 - \bar{E}_2)t + i\theta_v} + \text{c.c.}] \end{aligned}$$

$$\begin{aligned} &\approx c_1^2 e^{-\bar{\Gamma}_1 t} + 2c_1 c_2 \langle v_1 | v_2 \rangle |e^{-\frac{\bar{\Gamma}_1 + \bar{\Gamma}_2}{2} t} \\ &\times \cos[(\bar{E}_1 - \bar{E}_2)t + \theta_v], \end{aligned} \quad (\text{D2})$$

where θ_v is the relative phase of the eigenvectors $|v_1\rangle$ and $|v_2\rangle$. The damping behaviors of $w(t)$ are determined by the term $c_1^2 e^{-\bar{\Gamma}_1 t} + 2c_1 c_2 \langle v_1 | v_2 \rangle |e^{-\frac{\bar{\Gamma}_1 + \bar{\Gamma}_2}{2} t}$, marked as p_d . The damping curve $w_d(t)$ is thus

$$\begin{aligned} w_d(t) &= -\frac{\partial_t p_d}{p_d} = \bar{\Gamma}_1 - \frac{\bar{\Gamma}_1 - \bar{\Gamma}_2}{2} \frac{1}{1 + \frac{c_1^2}{A'} e^{-\frac{\bar{\Gamma}_1 - \bar{\Gamma}_2}{2} t}} \\ &\approx \bar{\Gamma}_1 - \frac{\bar{\Gamma}_1 - \bar{\Gamma}_2}{2} \frac{1}{\frac{c_1^2}{A'} e^{-\frac{\bar{\Gamma}_1 - \bar{\Gamma}_2}{2} t}} \\ &= \bar{\Gamma}_1 - \frac{\bar{\Gamma}_1 - \bar{\Gamma}_2}{2} \frac{A'}{c_1^2} e^{-\frac{\bar{\Gamma}_1 - \bar{\Gamma}_2}{2} t} \\ &\equiv A e^{-\frac{\bar{\Gamma}_1 - \bar{\Gamma}_2}{2} t} + \bar{\Gamma}_1 = A e^{-\frac{\gamma_1^1 - \gamma_1^0}{2} t} + \gamma_1^0, \end{aligned} \quad (\text{D3})$$

where $A' \equiv 2c_1 c_2 \langle v_1 | v_2 \rangle$.

- [1] P. Eckle, A. N. Pfeiffer, C. Cirelli, A. Staudte, R. Dörner, H. G. Muller, M. Büttiker, and U. Keller, *Science* **322**, 1525 (2008).
- [2] P. Eckle, M. Smolarski, P. Schlup, J. Biegert, A. Staudte, M. Schöffler, H. G. Muller, R. Dörner, and U. Keller, *Nat. Phys.* **4**, 565 (2008).
- [3] A. N. Pfeiffer, C. Cirelli, M. Smolarski, D. Dimitrovski, M. Abu-samha, L. B. Madsen, and U. Keller, *Nat. Phys.* **8**, 76 (2012).
- [4] A. S. Landsman, M. Weger, J. Maurer, R. Boge, A. Ludwig, S. Heuser, C. Cirelli, L. Gallmann, and U. Keller, *Optica* **1**, 343 (2014).
- [5] N. Camus, E. Yakaboylu, L. Fechner, M. Klaiber, M. Laux, Y. Mi, K. Z. Hatsagortsyan, T. Pfeifer, C. H. Keitel, and R. Moshhammer, *Phys. Rev. Lett.* **119**, 023201 (2017).
- [6] U. S. Sainadh, H. Xu, X. Wang, A. Atia-Tul-Noor, W. C. Wallace, N. Douguet, A. Bray, I. Ivanov, K. Bartschat, A. Kheifets, R. T. Sang, and I. V. Litvinyuk, *Nature (London)* **568**, 75 (2019).
- [7] L. Torlina, F. Morales, J. Kaushal, I. Ivanov, A. Kheifets, A. Zielinski, A. Scrinzi, H. G. Muller, S. Sukiasyan, M. Ivanov, and O. Smirnova, *Nat. Phys.* **11**, 503 (2015).
- [8] L. V. Keldysh, *Sov. Phys. JETP* **20**, 1307 (1965).
- [9] F. H. M. Faisal, *J. Phys. B* **6**, L89 (1973).
- [10] H. R. Reiss, *Phys. Rev. A* **22**, 1786 (1980).
- [11] C. R. McDonald, G. Orlando, G. Vampa, and T. Brabec, *Phys. Rev. Lett.* **111**, 090405 (2013).
- [12] E. E. Serebryannikov and A. M. Zheltikov, *Phys. Rev. Lett.* **116**, 123901 (2016).
- [13] M. Klaiber and J. S. Briggs, *Phys. Rev. A* **94**, 053405 (2016).
- [14] L. Sarkadi, *J. Phys. B: At. Mol. Opt. Phys.* **53**, 165401 (2020).
- [15] L. Jia, H. Xing, and L. Fu, *Phys. Rev. A* **106**, 022814 (2022).
- [16] M. Drescher, M. Hentschel, R. Kienberger, M. Uiberacker, V. Yakovlev, A. Scrinzi, T. Westerwalbesloh, U. Kleineberg, U. Heinzmann, and F. Krausz, *Nature (London)* **419**, 803 (2002).
- [17] M. Uiberacker, T. Uphues, M. Schultze, A. J. Verhoef, V. Yakovlev, M. F. Kling, J. Rauschenberger, N. M. Kabachnik, H. Schröder, M. Lezius, K. L. Kompa, H.-G. Muller, M. J. J. Vrakking, S. Hendel, U. Kleineberg, U. Heinzmann, M. Drescher, and F. Krausz, *Nature (London)* **446**, 627 (2007).
- [18] E. Goulielmakis, Z.-H. Loh, A. Wirth, R. Santra, N. Rohringer, V. S. Yakovlev, S. Zherebtsov, T. Pfeifer, A. M. Azzeer, M. F. Kling, S. R. Leone, and F. Krausz, *Nature (London)* **466**, 739 (2010).
- [19] H. Wang, M. Chini, S. Chen, C.-H. Zhang, F. He, Y. Cheng, Y. Wu, U. Thumm, and Z. Chang, *Phys. Rev. Lett.* **105**, 143002 (2010).
- [20] M. Holler, F. Schapper, L. Gallmann, and U. Keller, *Phys. Rev. Lett.* **106**, 123601 (2011).
- [21] M. Sabbar, H. Timmers, Y.-J. Chen, A. K. Pymer, Z.-H. Loh, S. G. Sayres, S. Pabst, R. Santra, and S. R. Leone, *Nat. Phys.* **13**, 472 (2017).
- [22] N. Eicke and M. Lein, *Phys. Rev. A* **97**, 031402(R) (2018).
- [23] I. A. Ivanov, C. Hofmann, L. Ortmann, A. S. Landsman, C. H. Nam, and K. T. Kim, *Commun. Phys.* **1**, 81 (2018).
- [24] N. Douguet and K. Bartschat, *Phys. Rev. A* **97**, 013402 (2018).
- [25] H. Ni, U. Saalman, and J.-M. Rost, *Phys. Rev. A* **97**, 013426 (2018).
- [26] H. Ni, U. Saalman, and J.-M. Rost, *Phys. Rev. Lett.* **117**, 023002 (2016).

- [27] H. Ni, N. Eicke, C. Ruiz, J. Cai, F. Oppermann, N. I. Shvetsov-Shilovski, and L.-W. Pi, *Phys. Rev. A* **98**, 013411 (2018).
- [28] P. B. Corkum, *Phys. Rev. Lett.* **71**, 1994 (1993).
- [29] M. Lewenstein, P. Balcou, M. Y. Ivanov, A. L'Huillier, and P. B. Corkum, *Phys. Rev. A* **49**, 2117 (1994).
- [30] A. W. Bray, S. Eckart, and A. S. Kheifets, *Phys. Rev. Lett.* **121**, 123201 (2018).
- [31] U. Fano, *Phys. Rev.* **124**, 1866 (1961).
- [32] S. Barnett and P. Radmore, *Methods in Theoretical Quantum Optics, Section 6.5* (Oxford University Press, 2002).
- [33] J. Vábek, H. Bachau, and F. Catoire, *Phys. Rev. A* **106**, 053115 (2022).
- [34] W. Magnus, *Comm. Pure Appl. Math.* **7**, 649 (1954).
- [35] I. I. Rabi, *Phys. Rev.* **51**, 652 (1937).
- [36] W.-C. Jiang, H. Liang, S. Wang, L.-Y. Peng, and J. Burgdörfer, *Phys. Rev. Res.* **3**, L032052 (2021).